Journal of Materials Chemistry C

Accepted Manuscript

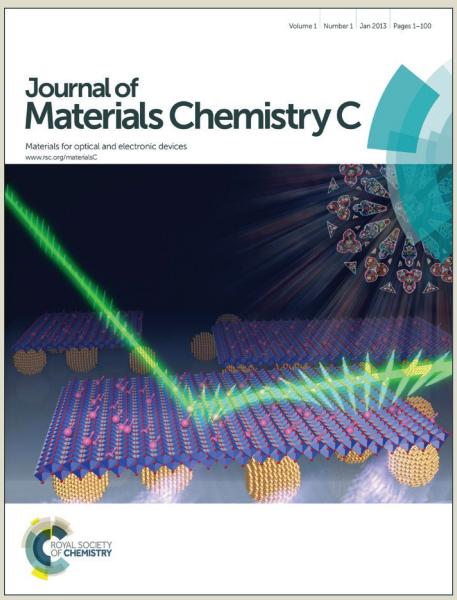

ROYAL SOCIETY OF CHEMISTRY

www.rsc.org/materialsC

Journal Name

ARTICLE

Structure and Local Polar Domains of Dy-Modified $BiFeO_3$-$PbTiO_3$ Multiferroic Solid Solution

Received 00th January 20xx,
Accepted 00th January 20xx

DOI: 10.1039/x0xx00000x

www.rsc.org/

Jian Zhuang,[a,b] Lun-Wei Su,[b] Hua Wu,[c,b] Alexei A. Bokov,[b] Wei Ren[†a] and Zuo-Guang Ye [†b,a]

To investigate the effects of dysprosium ion on the crystal structure and multiferroic properties of the bismuth ferrite-based systems, Dy-substituted solid solutions of $0.66Bi_{1-x}Dy_xFeO_3$-$0.34PbTiO_3$, with x = 0, 0.05, 0.1, 0.15, 0.2, 0.3, 0.4 and 0.5, have been synthesized and characterized. With increasing concentration of Dy, the crystal structure transforms from a primarily tetragonal P4mm phase to a rhombohedral R3c phase. Moreover, a small amount of the R3c (or monoclinic Cc) phase is found to coexist with the P4mm phase in the composition range of $0 \le x < 0.2$, which is attributed to the effect of Dy that favours the rhombohedral structure. Interestingly, the ferroelectric phase transition temperature T_C increases with increasing Dy concentration for compositions with $x \ge 0.1$. This is explained by the crystal structural effect that compensates the dilution effect of the ferroelectrically active Bi^{3+}. Piezoresponse Force Microscopy (PFM) imaging reveals the formation of 180° polar domains, which can be switched by applying electric fields through the PFM tip, confirming the ferroelectricity. A partial phase diagram is established in terms of composition and temperature. It describes the crystal structure and ferroelectric phases, as well as the solubility limit, of the $Bi_{1-x}Dy_xFeO_3$-$PbTiO_3$ solid solution system.

1. Introduction

Magnetoelectric multiferroic materials have drawn a lot of attentions due to the coexistence of ferroelectric and magnetic orders and the coupling between them. As one of the most promising room temperature single phase multiferroic materials, $BiFeO_3$ (BFO) possesses a giant polarization with a high ferroelectric Curie temperature (T_C) of ~ 1100 K, and an antiferromagnetic structure with a Néel temperature around 643 K. Experimental and theoretical studies[1-3] indicate that its polarization along the <111> direction is in the order of 90 – 100 $\mu C/cm^2$. However, there are still some serious obstacles that need to be overcome before the potential practical applications of BFO in highly promising magnetoelectric memories, spintronic devices, etc., could be realized.[1, 4, 5] First, the synthesis of pure BFO bulk material is difficult due to the unstable nature of the perovskite phase above 948 K during the solid state reaction and sintering process. Second, the large leakage current due to the existence of the mixed-valence Fe^{2+}/Fe^{3+} ions and oxygen vacancies makes it difficult, if not impossible, to display the intrinsic excellent ferroelectric properties. Third, BFO lacks ferromagnetic ordering due to cycloid-modulated antiferromagnetic arrangement of the spins which only results in an antiferromagnetic ordering at room temperature.[6]

A great deal of effort has been made to resolve these issues. Many chemically modified $BiFeO_3$–based bulk materials were reported with enhanced ferroelectric and ferromagnetic properties.[5,7-15] Among these materials, the solid solution of $(1–x)BiFeO_3–xPbTiO_3$ (BF–PT) has proved to be of particular interests as it can be formed in a stable perovskite phase by solid state reaction and exhibits a morphotropic phase boundary (MPB) approximately at x = 0.3.[15–18] In our previous work,[19-21] the magnetic ion Dy^{3+} has been introduced to the BF–PT system to form the $(1–x)[0.9BiFeO_3–0.1DyFeO_3]–xPbTiO_3$ (BDF–xPT) pseudo–binary solid solution in order to further improve the multiferroic properties. It was shown that the BDF–xPT ceramics of compositions within the MPB demonstrate simultaneously good ferroelectricity and weak-ferromagnetism at room temperature. However, as the substitution amount of Dy was kept constant (x = 0.10), it was not possible to investigate the effects of Dy on the structure and properties of the $BiFeO_3$-$PbTiO_3$ (BF-PT) system , and the mechanisms of the property-enhancement. Given the significant interests in this multiferroic systems, it became naturally important and necessary to study the BF-PT system with different substitution amounts of Dy.

In this work, we have systematically studied the new solid solution system of $0.66Bi_{1-x}Dy_xFeO_3$-$0.34PbTiO_3$ with different Dy substituting concentrations, with a view to investigating the intricate effects of Dy on the structure and properties of BF-PT. The $0.66Bi_{1-x}Dy_xFeO_3$-$0.34PbTiO_3$ ceramics have been prepared and characterized by X-ray diffraction, dielectric measurements and piezoresponse force microscopy. The effects of Dy-substitution for Bi on the crystal symmetry, local polar domains, and dielectric and ferroelectric properties are discussed in detail. The results of this work have shed light on how the substitution of Dy can affect the

[a] Electronic Materials Research Laboratory, Key Laboratory of the Ministry of Education & International Center for Dielectric Research, Xi'an Jiaotong University, Xi'an, 710049, P. R. China.
[b] Department of Chemistry and 4D LABS, Simon Fraser University, Burnaby, British Columbia, V5A 1S6, Canada.
[c] Department of Applied Physics, Donghua University, Ren Min Road 2999, Songjiang District, 201620 Shanghai, P. R. China.
† Zuo-Guang Ye(zye@sfu.ca), Wei Ren(wren@mail.xjtu.edu.cn)

structural symmetry and properties of the $BiFeO_3$-based multiferroic solid solution.

2. Experiment

The Dy-substituted solid solutions of $0.66Bi_{1-x}Dy_xFeO_3$-$0.34PbTiO_3$, with x=0, 0.05, 0.10, 0.15, 0.20, 0.30, 0.40, and 0.50, were synthesized in the form of ceramics by solid state reaction and sintering process. The samples are named after their compositions, e.g., Dy05 stands for $0.66Bi_{0.95}Dy_{0.05}FeO_3$-$0.34PbTiO_3$, Dy10 stands for $0.66Bi_{0.90}Dy_{0.10}FeO_3$-$0.34PbTiO_3$, and so on. The raw compounds of Fe_2O_3 (≥99.7%), Dy_2O_3 (99.9%), Bi_2O_3 (≥99%), PbO (≥99%) and TiO_2 (≥99%) were dried overnight and then weighed in stoichiometric amounts and mixed together. After hand-grinding the mixture in dilute ethanol for 1 h, the mixed powder was dried and pressed into pellets with a diameter of Φ = 15 mm. The pellets were subsequently calcined at 1123 K for 6 hrs in an alumina crucible. The calcined samples were then crushed into powder and reground thoroughly. The powder was mixed with 5 wt% polyvinyl alcohol (PVA) binder and pressed into pellets of Φ = 10mm. The pellets were heated at 773 K for 0.5 hrs to eliminate the PVA binder and then sintered at different temperatures from 1303 K to 1373 K for 2 hrs depending on the different compositions. Powder X-ray diffraction was performed using a Bruker D8 Advance Diffractometer to investigate the crystal structure. The phase components and lattice parameters were analyzed and calculated based on the Rietveld refinement method using Topas Academic Software package. The temperature variation of the dielectric constant was measured from room temperature up to 973 K at frequencies from 100 kHz to 1 MHz using a precision impedance analyzer (4294A, Agilent). The polar domain configurations and switching, and the piezoresponse under electric fields were studied on as-sintered ceramic samples by Piezoresponse Force Microscopy (PFM, Dimension Icon, NanoScope V, Bruker).

3. Results and Discussion

3.1 Structural Characterization

The room temperature powder X-ray diffraction (XRD) patterns of the different compositions of the $0.66Bi_{1-x}Dy_xFeO_3$-$0.34PbTiO_3$ solid solution are shown in Fig. 1(a). The Dy00 sample shows a dominant tetragonal phase characterized by the split of such peaks as $(100)_{pc}$, $(110)_{pc}$, etc., with a trace amount of rhombohedral phase, which is consistent with the results reported in Ref [17]. The details of the (110) peaks of selected compositions across the tetragonal and the rhombohedral phases are shown in Fig. 1(b). With the substitution of Dy for Bi, the rhombohedral phase component increases and gradually becomes the majority phase. For the compositions with x > 0.15, the splitting of diffraction peaks characteristic of the tetragonal phase eventually disappears and the structure transforms into a pure rhombohedral phase. It is noted that the two splitting (110) peaks in the rhombohedral phase are very close to, and overlap, each other, leading to the observed apparent broad single peak. This composition-induced transformation from the tetragonal to rhombohedral phase can be attributed to the effects of the substitution of Dy^{3+} ions for Bi^{3+} ions: the smaller size of Dy^{3+} causes rhombohedral distortion in the tetragonal lattice of BF-PT. Peaks arising from impurities are found to exist in Dy30, as indicated by solid circles in Fig. 1(a), and their intensity increases with the increasing amount of Dy, suggesting that the solubility limit of Dy into BF-PT is around x = 0.3. It is also worth noting that the sintered pellets of Dy00 and Dy05 self-disintegrated into powders when cooled down to room temperature. This implies the existence of huge internal strain developed inside the ceramic samples when undergoing the structural phase transition from the cubic phase to the tetragonal P4mm phase upon cooling at T_C, with a very large tetragonality (c/a ratio) (see below), which is characteristic of the BF-PT solid solution and its ceramics.[22]

The phase components are analyzed and the lattice parameters are calculated using the Rietveld refinement method. The variations of the lattice parameters as a function of composition are plotted in Fig. 1(c). The dominant tetragonal phase for the compositions with

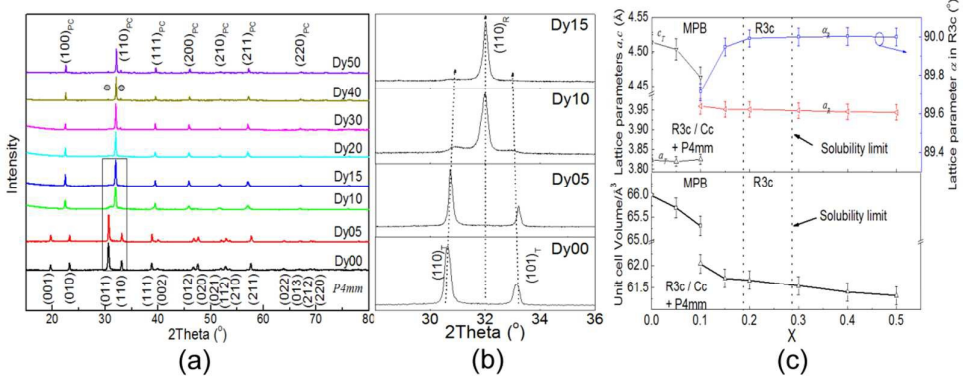

Fig. 1. (a) Room temperature XRD patterns of the $0.66Bi_{1-x}Dy_xFeO_3$-$0.34PbTiO_3$ solid solution of different compositions, (b) Enlarged (110) peaks for selected compositions and (c) Variations of lattice parameters and unit cell volume as a function of composition x, as well as the phase components.

x < 0.1 can be indexed with the P4mm symmetry while the major rhombohedral phase of the compositions with x > 0.1 can be indexed with the R3c symmetry. However, the phase components of the composition with x = 0.1 in which the amounts of the tetragonal and rhombohedral phases are comparable, appear to be complex. Two combinations of phase, i.e. (P4mm + R3c) and (P4mm + Cc), were found to be possible according to our previous results.[20] As x increases, the c/a ratio of the P4mm phase decreases from 1.181 for Dy00 to 1.167 for Dy10, indicating a decrease of the tetragonality and thereby the degradation of the P4mm phase. With further increase in x, the lattice parameter a_R of the R3c phase decreases and the angle α approaches 90°. As shown in Fig. 1(c), the unit cell volumes of both phases continue to decrease with increasing x, which is also caused by the substitution of the smaller guest ion of Dy^{3+} for the relatively big host ion of Bi^{3+}.

The nature of the MPB in the BF-PT ceramics was reported to be metastable,[23] i.e. R3c is a metastable phase while P4mm is an equilibrium structure for the compositions with a PT concentration > 0.27, and vice versa for the compositions with a PT concentration < 0.27. According to this, the equilibrium phase in the Dy00 sample ($0.66BiFeO_3$-$0.34PbTiO_3$) investigated here is the tetragonal phase while R3c is the metastable phase. The structural transition from P4mm to R3c induced by the Dy-substitution suggests that the equilibrium phase changes from P4mm to R3c with the increasing amount of Dy. The critical composition separating two different equilibrium phases is around x = 0.1, above which the R3c phase becomes prevailing. In fact, similar structural transition from P4mm to R3c is also observed in the La-doped BF-PT ceramics.[24] Considering that the R3c metastable phase can be present only if the R3c nuclei do not vanish completely when cooling down from the sintering temperature,[25] it is possible that the substitution of Dy^{3+} or La^{3+} can influence the surrounding unit cells by forming local rhombohedral distortion, which could act as the nuclei for the R3c phase. These rhombohedral nuclei are believed to be more stable and have a longer lifetime than the metastable components in the unsubstituted samples, favouring the formation of the R3c phase. It is also worth noting that the rhombohedral distortion decreases with increasing Dy content when x > 0.1, as shown in Fig. 2 (c). This can be explained as follows: on the one hand, Dy can promote the formation of a stable R3c phase in the BF-PT matrix. On the other hand, the addition of Dy reduces the amount of Bi and thereby weakens the rhombohedral distortion of the BF-PT matrix. As a result of these competing effects, the overall rhombohedral distortion decreases with increasing Dy concentration when x > 0.1. Although a mixture of the phases is present in a wide composition range due to the existence of metastable phases, the stable MPB region is believed to be around x = 0.1.

3.2 Phase Transition

The temperature dependence of the dielectric constant (ε-T) is measured from room temperature to 973 K at the frequency of 1 kHz for the $0.66Bi_{1-x}Dy_xFeO_3$-$0.34PbTiO_3$ ceramics with x = 0.10, 0.15, 0.20 and 0.30 (the compositions with x = 0 and 0.05 cannot form dense ceramics to carry out dielectric measurements, as they break down upon cooling), and the results are shown in Fig. 2. A sharp and strong dielectric peak appears for all the samples investigated, which indicates the structural phase transition from the ferroelectric phase

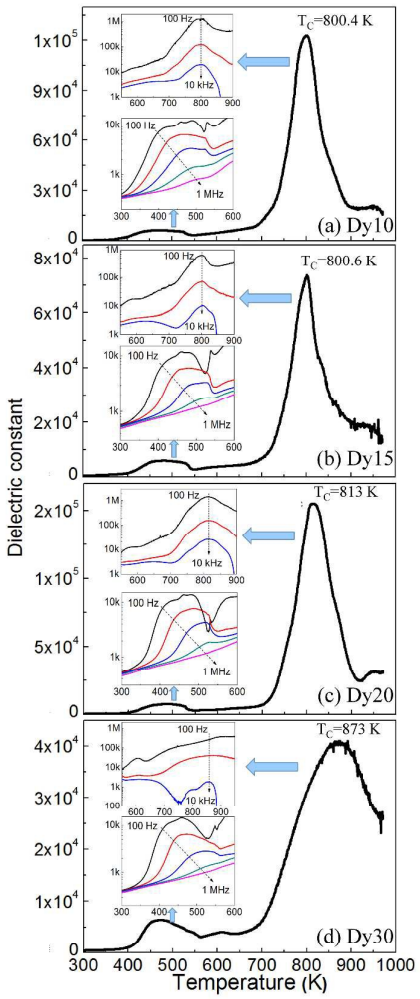

Fig. 2. Temperature dependence of the dielectric constant (ε-T) of different compositions of the $0.66Bi_{1-x}Dy_xFeO_3$-$0.34PbTiO_3$ ceramics: (a) Dy10, (b) Dy15, (c) Dy20 and (d) Dy30. The insets show the ε-T curves at different frequencies around the relaxation peak (lower) and the dielectric maximum (i.e. T_C, upper).

to the cubic phase. The ε-T curves around the dielectric maximum at different frequencies are plotted and presented in the upper set of insets in Fig. 2. The Curie temperature T_C is found to be generally frequency independent within the measurement errors. Also, it is also worth noting that the significantly increasing contribution of leakage at high temperature leads to a large dielectric loss and thereby very broad and faint phase transition peaks, and makes it difficult to analyze the possible relaxation behaviours. The T_C of this transition increases with increasing substituting amount of Dy, from 800.4 K for DF10 to around 873 K for DF30 at 1 kHz. On the one hand, with increasing Dy content, the concentration of ferroelectrically active Bi^{3+} ions decreases, which would lead to a decreased polarization and consequently a reduced T_C. On the other hand, the substitution of Dy for Bi drives the structure from P4mm into R3c, as discussed in Sec. 3.1. In these two competing processes, the latter prevails, i.e. the ferroelectric ordering in rhombohedral phase must

be more stable and stronger than that in the P4mm phase, giving rise to a higher T_C for the Dy-substituted rhombohedral phase. Although the "rhombohedral" distortion decreases due to the decreasing amount of Bi, the R3c phase becomes increasingly stable with increasing concentration of Dy, leading to an overall increase in T_C for compositions with $x \geq 0.1$. Note that, without the addition of Dy, the T_C of Dy00 was reported to be in the range of 874 K – 905 K, [26] which is higher than the DF10 sample studied here. This suggests that the diluting effect of the Bi^{3+} ions is predominant in the compositions with a low concentration of Dy, i.e. $x < 0.1$, leading to an overall decrease in T_C.

A small and broad bump is present around 473 K for all the compositions studied, as shown in the lower set of insets in Fig. 2. In order to investigate the nature of this dielectric anomaly, the dielectric constant is measured at different frequencies from 100 Hz to 1 MHz in the temperature range of 300 K – 600 K. The dielectric maximum shifts to higher temperatures while its magnitude decreases sharply as the frequency increases, and the bump disappears at 1 MHz. This behaviour indicates a characteristic dielectric relaxation process rather than a relaxor behaviour, which is probably caused by the existence of mobile charges or defects. The detailed mechanism of this relaxation is under investigation.

3.3 Polar Domain Structure and Local Piezoresponse

The polar domain structure and local piezoresponse of the Dy-substituted BF-PT ceramics are investigated by PFM, and the results are presented in Fig. 3. Columns (I) and (III) of Fig. 3 show the PFM images of Dy15 and Dy20, respectively, in terms of (a) topography, (b) out–of–plane piezoresponse phase images, (c) out–of–plane piezoresponse amplitude images, (d) in–plane piezoresponse phase images, and (e) in–plane piezoresponse amplitude images, of a 3 μm×3 μm area. In the out–of–plane phase images presented in Figs. 3(b), the dark and bright areas reveal the polar domains with polarizations directed upward (⊙) and downward (⊕), respectively, perpendicularly to the surface. In the in–plane piezoresponse phase images shown in Figs. 1(d), the dark and bright regions correspond to the two in–plane polarization components of opposite directions (← and →). The brightness in Figs. 3(c) and (d) represents the piezoresponse amplitude. In Fig. 3(a), both the Dy15 and Dy20 samples exhibit clear boundaries between grains. The surface roughness is within 500 nm in the scanned area.

As a natural pining source of domains, the grain boundaries are known to serve as domain walls as well.[20] On average, the domain size is of micron dimension in Fig. 3(I). Within one grain, two kinds of domains can be found and the domain walls are irregular, indicating the formation of 180° polar domains between them. In addition, the in-plane piezoresponse signal is found to be stronger than that of the out-of-plane piezoresponse. This suggests that the

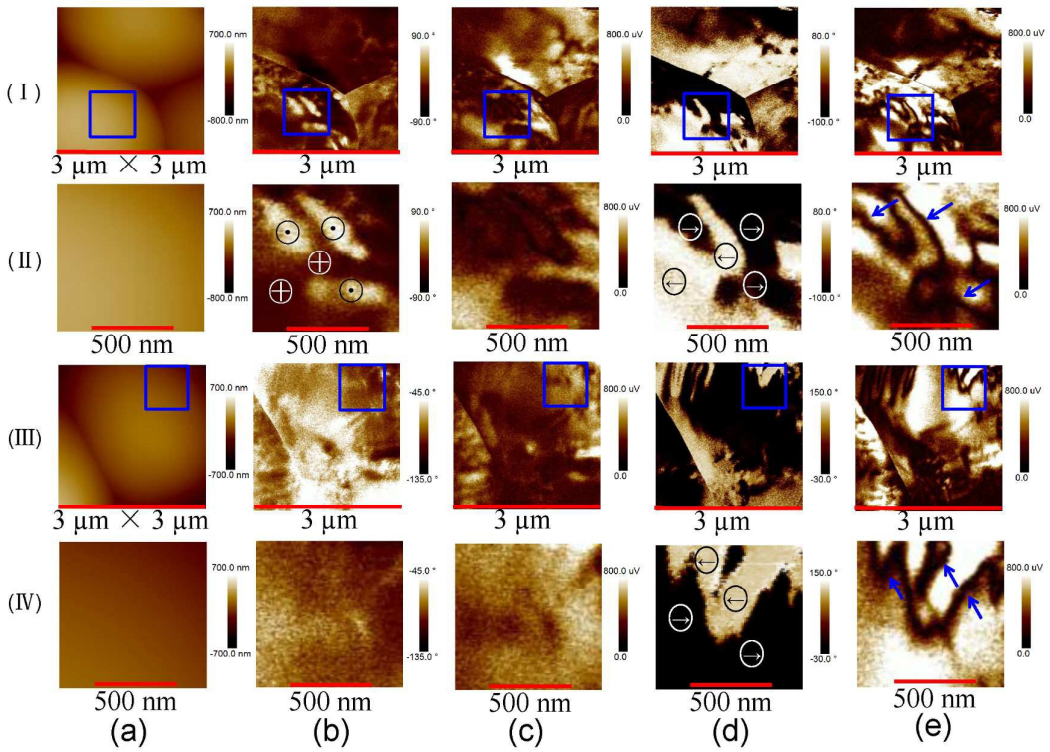

Fig. 3. PFM images of as–sintered ceramic surface of (I) Dy15, (II) selected area of Dy15, (III) Dy20 and (IV) selected area of Dy20, in terms of (a) Topography, (b) Out–of–plane PFM phase images, (c) Out–of–plane PFM amplitude images, (d) In–plane PFM phase images, and (e) In–plane PFM amplitude.

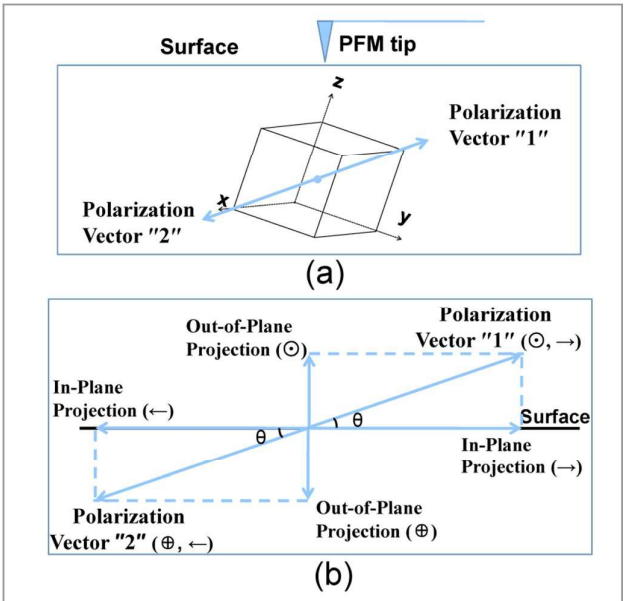

Fig. 4. Schematics of a pair of rhombohedral polarization vectors (a), giving rise to stronger in-plane polarization components and thereby piezoresponse amplitude than the out-of-plane counterparts (b).

polarization vector contributes a larger component to the in-plane direction than to the out-of-plane direction. Given the major rhombohedral symmetry in Dy15, the observed domains and polarization orientation could arise from the pair of polarization vectors "1" and "2" forming an acute angle with the in-plane directions that are dominant over the three other pairs of the rhombohedral polarization vectors, as shown by the sketch in Fig. 4(a). The resulting piezoresponse is explained in Fig. 4(b). It can be seen that the polarization vector "1" gives rise to the piezoresponse of (⊙, →), while the polarization vector "2" gives rise to the piezoresponse of (⊕, ←). The angle θ determines the relative strength of the in-plane and out-of-plane piezoresponse, and an acute angle θ gives rise to a larger in-plane projection and a smaller out-of-plane projection, as observed in Fig. 3(I).

In order to examine the domain structure and orientation of Dy15 in more detail, the PFM images of a selected area, indicated by the square in Fig. 3(I), is magnified and shown in Fig. 3(II). It can be seen that the in-plane (Fig. 3(II, b)) and out-of-plane (Fig. 3(II, d)) domains generally show similar and correlated domain configurations, i.e., most of the in-plane domains with the "←" polarization orientation correspond to the out-of-plane domains with the "⊕" orientation (from polarization vector "2"), while most of the in-plane domains with the "→" polarization orientation are coupled to the out-of-plane domains with the "⊙" orientation (from polarization vector "1"). This is consistent with the explanation given in Fig. 4(b), and confirms the formation of 180° polar domains. In piezoresponse amplitude images in Fig. 3(II, e), irregular domains walls with almost zero amplitude are clearly observed, as indicated by arrows, which are also characteristic of 180° polar domains.

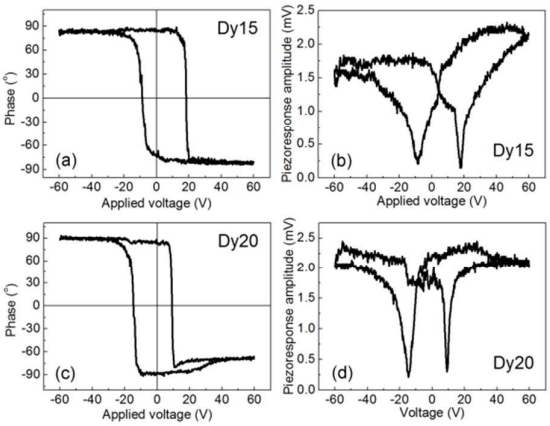

Fig. 5. Piezoresponse phase and amplitude of the Dy15 (a, b) and Dy20 (c, d) ceramics, under an AC electric field.

Similar to Dy15, the PFM images of Dy20 shows clear in-plane 180° domains with micron dimension (Fig. 3(III)). The magnified and detailed domain configurations of a selected square area in Fig. 3(c) are shown in Fig. 3(IV). The in-plane domain patterns are clearly displayed while no obvious out-of-plane signal can be observed, indicating that the polarization components are mainly along the in-plane directions, i.e., the angle θ of the corresponding polarization vector is close to 0° (Fig. 4(b)). Additionally, some cuneate-like in-plane domains are observed. Also, in-plane domain walls with a near-zero piezoresponse amplitude are clearly imaged in Fig. 3(IV, e), as indicated by arrows.

The local piezoresponse under an applied electric field is probed by applying an AC voltage of ± 60 V on the sample via the PFM tip while the sample is grounded. The electric field dependences of the piezoresponse phase and amplitude of Dy15 are shown in Fig. 5(a) and (b), respectively. It can be seen that the phase changes from a

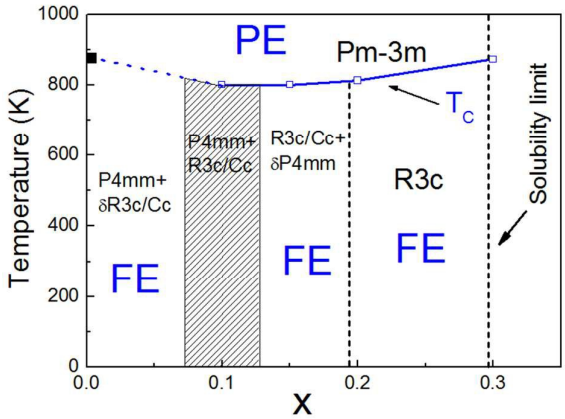

Fig. 6. (Partial) Phase diagram of the $0.66Bi_{1-x}Dy_xFeO_3$-$0.34PbTiO_3$ solid solution system. The phase transition temperature of the Dy00 sample is taken from the Ref [23].

positive to negative value when the applied field changes its polarity, indicating that the local polar domains can be poled and switched by the electric field. The difference between the negative and positive phases is close to 180°, which is characteristic of the switching of two polar domains with opposite polarizations. The piezoresponse amplitude exhibits a butterfly-shaped variation as a function of the electric field, as displayed in Fig. 5(b), indicative of local piezoelectricity associated to the polarization switching. Note that the coercive fields for the domain switching are about +20 V and -10V. Such asymmetrical domain switching could be caused by internal bias fields. The Dy20 ceramic shows similar behaviour of piezoresponse under an external field with its phase and amplitude shown in Fig. 5(c) and (d). The switching of polar domains and the associate piezoresponse confirm the existence of ferroelectricity in the Dy-substituted BF-PT solid solution.

3.4 Phase Diagram

Based on the results obtained above, a partial phase diagram is established for the $0.66Bi_{1-x}Dy_xFeO_3$-$0.34PbTiO_3$ solid solution in term of temperature and composition, as shown in Fig. 6. It depicts the effects of Dy-substitution on the phase symmetry and components, phase transition temperature and ferroelectric property of BF-PT. With the increase of Dy concentration, the phase symmetry changes from the tetragonal P4mm phase to the rhombohedral R3c phase with $x \geq 0.20$. While a mixture of phases is found in a wide composition range of $0 \leq x < 0.2$, a morphotropic phase boundary region can be identified in which the tetragonal P4mm and rhombohedral R3c (or monoclinic Cc) phase coexist in comparable amount, as represented by the shaded area. The polar nature and ferroelectricity of the low-temperature phases are found in BF-PT[15, 27] and in the Dy-substituted samples.

Conclusions

Dy-modified solid solution of $0.66BiFeO_3$-$0.34PbTiO_3$ has been synthesized in the form of ceramics using solid state reaction method. With increasing substitution amount of Dy, the crystal structure changes from a primarily tetragonal P4mm phase to the stable rhombohedral R3c phase, suggesting that the substitution of Dy for Bi can stabilize the R3c symmetry and hinder the formation of the P4mm phase. The unit cell volume shows a general decrease with increasing Dy content due to the relative small radius of Dy^{3+} compared with Bi^{3+}. Interestingly, with increasing concentration of Dy, the ferroelectric phase transition temperature T_C first decreases for compositions with $x < 0.1$ and then increases for compositions with $x \geq 0.1$. This is explained by the competition between two processes arising for the Dy-substitution: the effect of the dilution of the ferroelectrically active Bi^{3+} ion which would reduce T_C, and the effect of the structural transformation from the P4mm phase to the R3c phase with a more stable ferroelectric ordering and thereby increased T_C. The former is dominant in the compositions with $x < 0$, resulting in a slight decrease in T_C, while the latter prevails in the compositions with $x \geq 0.1$, giving rise to an increase in T_C. Piezoresponse Force Microscopy (PFM) imaging reveals the formation of 180° polar domains for the Dy15 and Dy20 samples, which can be poled and switched by applying an electric field through the PFM tip, confirming the ferroelectricity. A partial phase diagram is established in terms of composition and temperature, which depicts the crystal structure and ferroelectric phases, as well as the solubility limit, of the $0.66Bi_{1-x}Dy_xFeO_3$-$0.34PbTiO_3$ solid solution system. The results of this work show that the substitution of Dy can affect the structural symmetry and phase component of the $BiFeO_3$-based multiferroic solid solution, and thereby enhance its ferroelectric order, in addition to its effects on the magnetic and magnetoelectric properties which will be reported elsewhere.

Acknowledgements

This work was supported by the National Natural Science Foundation of China (Grant Nos. 50728201 and 90923001), the Intl. Sci. & Tech. Coop. Prog. of China (Grant No. 2011DFA51880), the "111 Project" of China (Grant No. B14040), the Natural Science and Engineering Council of Canada (NSERC) and the United States Office of Naval Research (ONR Grant No. N00014-12-1-1045). HW thanks the Fundamental Res. Funds for the Central Univ. for support. ZGY and WR acknowledge the "Qianren Program" and the "985 Project" of the Chinese Government for support.

Notes and references

1 J. Wang, J. B. Neaton, H. Zheng, V. Nagarajan, S. B. Ogale, B. Liu, D. Viehland, V. Vaithyanathan, D. G. Schlom, U. V. Waghmare, N. A. Spaldin, K. M. Rabe, M. Wuttig, and R. Ramesh, *Science*, 2003, **299**, 1719.
2 D. Lebeugle, D. Colson, A. Forget, and M. Viret, *Appl. Phys. Lett.,* 2007, **91**, 022907.
3 J. B. Neaton, C. Ederer, U. V. Waghmare, N. A. Spaldin, and K. M. Rabe, *Phys. Rev. B.,* 2005, **71**, 014113.
4 G. Catalan and J. F. Scott, Adv. Mater., 2009, **21**, 2463–2485.
5 V. M. Skorikov, A. N. Kalinkin, and A. E. Polyakov, *Inorg. Mater*., 2012, **48** (13), 1210–1225.
6 R. Safi and H. Shokrollahi, Prog, *Solid State Chem*., 2012, **40**, 6–15.
7 V. A. Khomchenko, D. A. Kiselev, M. Kopcewicz, M. Maglione, V. V. Shvartsman, P. Borisov, W. Kleemann, A. M. L. Lopes, Y. G. Pogorelov, J. P. Araujo, R. M. Rubinger, N. A. Sobolev, J. M. Vieira, and A. L. Kholkin, *J. Magn. Magn. Mater*., 2009, **321**, 1692–1698.
8 D. H. Wang, W. C. Goh, M. Ning, and C. K. Ong, *Appl. Phys. Lett*., 2006, **88**, 212907.
9 W.-M. Zhu, L. W. Su, Z.-G. Ye, and W. Ren, *Appl. Phys. Lett*., 2009, **94**, 142908.
10 Q. H. Jiang, J. Ma, Y. H. Lin, and C.-W. Nan, *Appl. Phys. Lett*., 2007, **91**, 022914.
11 K. Ueda, H. Tabata, and T. Kawai, *Appl. Phys. Lett*., 1999, **75**(4), 555 – 557.
12 G. L. Yuan and S. W. Or, *J. Appl. Phys.,* 2006, **100**, 024109.
13 J. Walker, B. Budic, P. Bryant, V. Kurusingal, C. C. Sorrell, *IEEE Trans. Ultra. Ferro. Freq. Cont*., 2015, **62**, 83-87.
14 J. Walker, P. Bryant, V. Kurusingal, C. Sorrell, D. Kuscer, G. Drazic, A. Bencan, V. Nagarajan and T. Rojac, *Acta Materialia*, 2015, **83**, 149–159.
15 W.-M. Zhu and Z.-G. Ye, *Appl. Phys. Lett*., 2006, **89**, 232904.
16 S. Bhattacharjee and D. Pandey, *J. Appl. Phys.,* 2010, **107**, 124112.
17 W.-M. Zhu, H. Y. Guo, and Z.-G. Ye, *Phys. Rev. B*., 2008, **78**, 014401.
18 D. I. Woodward, I. M. Reaney, R. E. Eitel, and C. A. Randall, *J. Appl. Phys*., 2003, **94**(5), 3313 – 3318.

19 J. Zhuang, L. Chen, W. Ren, and Z.-G. Ye, *Ceram. Int*., 2013, **39**, S207–S211.
20 J. Zhuang, H. Wu, W. Ren, and Z.-G. Ye, *J. Appl. Phys*., 2014, **116**, 066809.
21 J. Zhuang, H. Wu, W. Ren, and Z.-G. Ye, *J. Appl. Phys*., 2015, **118**, 072005.
22 T.P.Comyn, T.Stevenson, M.Al-Jawad, S.L.Turner, R.I.Smith, W.G.Marshall, A.J. Bell, and R.Cywinski, *Appl. Phys. Lett*., 2008, **93**, 23.
23 V. Kothai, R. Prasath Babu, and R. Ranjan, *J. Appl. Phys*., 2013, **114**, 114102.
24 L. F. Cótica, F. R. Estrada, V. F. Freitas, G. S. Dias, I. A. Santos, J. A. Eiras, and D. Garcia, *J. Appl. Phys*., 2012, **111**, 114105 .
25 V. Kothai, A. Senyshyn, and R. Ranjan, *J. Appl. Phys*., 2013, **113**, 084102.
26 V. V. S.S. Sai Sunder, A. Halliyal, and A.M. Umarji, *J. Mater. Res*., 1995, 10, 5, pp. 1301-1306.
27 W-M. Zhu, H.-Y. Guo, and Z.-G. Ye, *J. Mater. Res.*, 2007, **22**(8), pp.2136-2143.